

Electronic Supplementary Information (ESI)

Hydrogen bond modulated molecular packing and its applications in high-performance non-doped organic electroluminescence

Yizhong Shi,^{‡a} Kai Wang,^{‡ad} Youichi Tsuchiya,^{def} Wei Liu,^{ad} Takeshi Komino,^d Xiaochun Fan,^a Dianming Sun,^a Gaole Dai,^a Jiaxiong Chen,^{ab} Ming Zhang,^c Caijun Zheng,^c Shiyun Xiong,^a Xuemei Ou,^a Jia Yu,^a Jiansheng Jie,^a Chun-Sing Lee,^{*b} Chihaya Adachi^{*def} and Xiaohong Zhang^{*a}

^a Institute of Functional Nano & Soft Materials (FUNSOM) and Jiangsu Key Laboratory for Carbon-Based Functional Materials & Devices, Soochow University, Suzhou, Jiangsu 215123, P. R. China

^b Center of Super-Diamond and Advanced Films (COSDAF) and Department of Chemistry, City University of Hong Kong, Hong Kong SAR, P. R. China

^c School of Optoelectronic Information, University of Electronic Science and Technology of China (UESTC), Chengdu, Sichuan 610054, P. R. China

^d Center for Organic Photonics and Electronics Research (OPERA) and Department of Applied Chemistry, Kyushu University, 744 Motooka, Nishi, Fukuoka 819-0395, Japan

^e JST, ERATO Adachi Molecular Exciton Engineering Project, Center for Organic Photonics and Electronics Research (OPERA), Kyushu University 744 Motooka, Nishi, Fukuoka 819-0395, Japan

^f International Institute for Carbon Neutral Energy Research (WPI-I2CNER), Kyushu University, 744 Motooka, Nishi, Fukuoka 819-0395, Japan

Corresponding Author

xiaohong_zhang@suda.edu.cn, apcslee@cityu.edu.hk, adachi@cstf.kyushu-u.ac.jp

Content

1. General Information.....	3
2. Synthesis	4
3. Results and Discussion	6
3.1 Theoretical simulations	6
3.2 Photophysical properties	6
3.3 Cyclic voltammograms.....	8
3.4 Device configuration	8
3.5 Single-crystal result	9
3.6 Spin density distributions (SDDs) of T₁ states.....	9
3.7 Atomic force microscopy (AFM) and XRD patterns	10
3.8 Carrier mobility	11
3.9 Transient PL measurements	12
3.10 TTA model	15
3.11 Variable angle spectroscopic ellipsometry (VASE) measurement	16
3.12 NMR charts.....	17
4. References.....	21

1. General Information

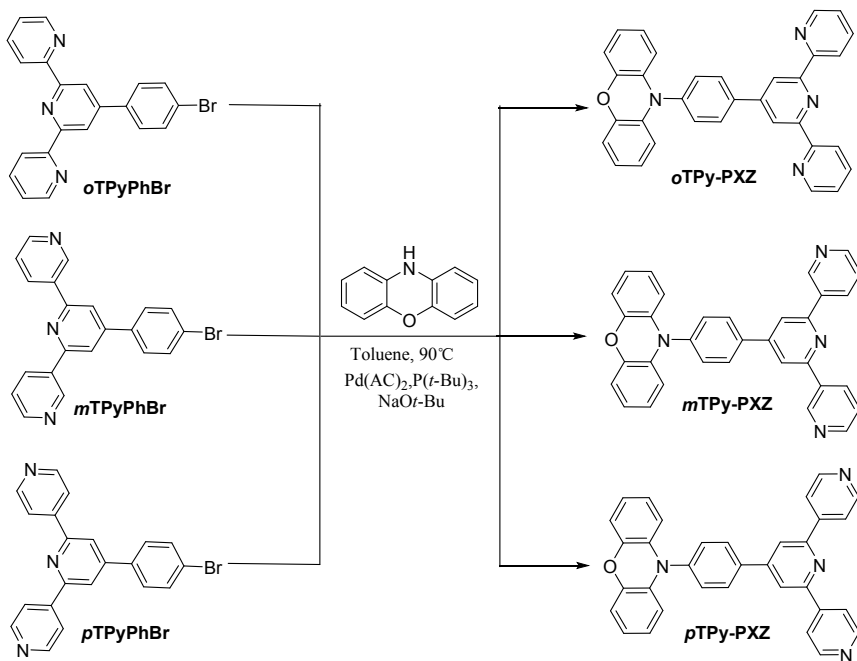
All reagents and starting materials were obtained from commercial suppliers and used without further purification. ^1H NMR and ^{13}C NMR spectra were recorded on a Bruker 400 spectrometer at room temperature. Mass spectrometry was performed with a Nermag R10-10C spectrometer. Single-crystal X-ray structure analysis was obtained using Bruker D8 Venture X-ray single crystal diffractometer. UV-vis absorption spectra were recorded on a Hitachi U-3900 spectrophotometer. PL spectra and phosphorescent spectra were recorded on a Hitachi F-4600 fluorescence spectrophotometer. PL quantum efficiency was measured by an absolute PL quantum yield measurement system (C11347-01, Hamamatsu Photonics) under the flow of nitrogen gas with an excitation wavelength of 300 nm. Emission lifetimes were measured using a streak camera (C4334, Hamamatsu Photonics) and cryostat (Iwatani Industrial Gases Co.) with a nitrogen gas laser (MNL200, Laser Technik) as an excitation light source under a pressure of about 3 Pa. Cyclic voltammetry (CV) was carried out on a CHI660e voltammetric analyzer at room temperature. Deaerated DMF was used as solvent with tetrabutylammonium hexafluorophosphate (TBAPF₆) (0.1 M) as the supporting electrolyte. The cyclic voltammograms (CV) were obtained at scan rate of 0.05 V·s⁻¹ with platinum electrode as the working/counter electrode and a saturated Ag/AgCl electrode as the reference electrode with standardized against ferrocene/ferrocenium.

The density functional theory (DFT) and time-dependent DFT (TD-DFT) calculations were performed by using Gaussian 09 with B3LYP/6-31g (d) basis set.^{1, 2} The spin-density distributions (SDDs) of the lowest excited triplet states were analyzed using a multifunctional wavefunction analyzer (Multiwfn 3.7)³ and visualized with VMD program (1.9.3).

The OLEDs were fabricated on the indium-tin oxide (ITO) coated transparent glass substrates, the ITO conductive layer has a thickness of ca. 100 nm and a sheet resistance of ca. 30 Ω per square. The substrates were cleaned with ethanol, acetone and deionized water, and then dried in an oven, finally exposed to UV ozone for 15 min. All the organic materials and metal layers were thermal evaporated under a vacuum of ca. 10⁻⁵ Torr. Four identical OLED devices were formed on each of the substrates and the emission area of 0.09 cm² for each device. The EL performances of the devices were measured with a PHOTO RESEARCH Spectra Scan PR 655 PHOTOMETER and a KEITHLEY 2400 Source Meter constant current source at room temperature.

2. Synthesis

The intermediate *o*TPyPhBr, *m*TPyPhBr and *p*TPyPhBr were synthesized by following experimental procedure described in previous report⁴ and used without further purification.



Scheme S1 Synthetic procedure of the three emitters.

Synthesis of 10-(4-([2,2':6',2"-terpyridin]-4'-yl) phenyl)-10H-phenoxazine (*o*TPy-PXZ):

Phenoxazine (384.7 mg, 2.10 mmol), *o*TPyPhBr (776.5 mg, 2.00 mmol), palladium(II) acetate (13.5 mg, 0.06 mmol), sodium tert-butoxide (576.6 g, 6.00 mmol) in a 100 mL two-necked flask, with stirring under argon atmosphere, was added tri-tert-butylphosphine (10 % in Toluene, 0.47 mL) and toluene (50 mL). The mixture was stirring at 90 °C for 12h. The cooled mixture was partitioned between EtOAc and water. The organic layer was separated, and the aqueous layer was extracted with EtOAc. The combined organic layers were washed with brine, dried over MgSO₄ and concentrated by rotary evaporator. The residue was purified by column chromatography on silica gel (eluent: EtOAc/THF=10/1) to afford *o*TPy-PXZ (820.5 mg, 83.63 %). ¹H NMR (400 MHz, CDCl₃, δ): 8.86 (s, 2H), 8.80 (m, 2H), 8.76 (d, J = 8.0 Hz, 2H), 8.24 – 8.14 (m, 2H), 7.96 (td, J = 7.7, 1.8 Hz, 2H), 7.60 – 7.52 (m, 2H), 7.44 (ddd, J = 7.5, 4.8, 1.2 Hz, 2H), 6.79 – 6.74 (m, 2H), 6.70 (ddd, J = 9.4, 7.5, 1.8 Hz, 4H), 6.09 – 5.99 (m, 2H); ¹³C NMR (101 MHz, CDCl₃, δ): 155.44, 155.37, 148.85, 148.50, 143.38, 139.16, 138.28, 136.51, 133.64, 130.82, 129.54, 123.44, 122.75, 120.88, 120.86, 118.52, 114.93, 112.71; HRMS (ESI) m/z: [M+H]⁺ calcd for C₃₃H₂₃N₄O 491.1794; found, 491.1790.

Synthesis of 10-(4-([3,2':6',3"-terpyridin]-4'-yl) phenyl)-10H-phenoxazine (*m*TPy-PXZ): *m*TPy-PXZ was synthesized by the same procedure using *m*TPyPhBr instead of *o*TPyPhBr. ¹H NMR (400 MHz, CDCl₃, δ): 9.41 – 9.40 (m, 2H), 8.80 – 8.68 (m, 2H), 8.54 (dt, J = 8.0, 1.9 Hz, 2H), 8.01 (s,

2H), 7.97 (d, J = 8.3 Hz, 2H), 7.55 (d, J = 8.3 Hz, 2H), 7.48 (ddd, J = 8.0, 4.8, 0.9 Hz, 2H), 6.72 (dd, J = 7.8, 1.6 Hz, 2H), 6.67 (td, J = 7.6, 1.5 Hz, 2H), 6.62 (td, J = 7.6, 1.6 Hz, 2H), 6.01 (dd, J = 7.9, 1.5 Hz, 2H); ^{13}C NMR (101 MHz, CDCl_3 , δ): 155.05, 149.73, 149.45, 147.79, 143.49, 139.85, 137.88, 134.23, 134.06, 133.56, 131.39, 129.43, 123.26, 122.81, 121.18, 117.28, 115.16, 112.76; HRMS (ESI) m/z: [M+H]⁺ calcd for $\text{C}_{33}\text{H}_{23}\text{N}_4\text{O}$ 491.1794; found, 491.1792.

Synthesis of 10-(4-([4,2':6',4'']-terpyridin]-4'-yl) phenyl)-10H-phenoxazine (*p*TPy-PXZ): *p*TPy-PXZ was synthesized by the same procedure using *p*TPyPhBr instead of *o*TPyPhBr. ^1H NMR (400 MHz, CDCl_3 , δ): 8.99 – 8.82 (m, 4H), 8.18 (m, 2H), 8.17 (m, 4H), 8.04 (d, J = 8.4 Hz, 2H), 7.63 (d, J = 8.4 Hz, 2H), 6.78 (td, J = 7.2, 6.7, 1.6 Hz, 2H), 6.74 (dd, J = 7.8, 1.6 Hz, 2H), 6.71 – 6.65 (m, 2H), 6.07 (dd, J = 7.8, 1.6 Hz, 2H); ^{13}C NMR (101 MHz, CDCl_3 , δ): 154.87, 149.85, 149.80, 149.66, 145.49, 143.43, 139.99, 137.49, 133.44, 131.40, 129.34, 122.70, 121.16, 120.70, 118.51, 115.13, 112.63; HRMS (ESI) m/z: [M+H]⁺ calcd for $\text{C}_{33}\text{H}_{23}\text{N}_4\text{O}$ 491.1794; found, 491.1792.

CCDC 1975855, 1975856 and 1975857 contains the supplementary crystallographic data for this paper. These data can be obtained free of charge from The Cambridge Crystallographic Data Centre via www.ccdc.cam.ac.uk/data_request/cif.

3. Results and Discussion

3.1 Theoretical simulations

Optimized ground state (S_0) geometries of three TADF isomers were estimated via the density functional theory (DFT) at the B3LYP/6-31G(d) level. As shown in Fig. S1, all emitters show highly twisted D-A conformations due to the typical steric hindrance, beneficial for effective HOMO-LUMO separations. And the LUMOs are mainly localized on the TPY moieties whereas the HOMOs are distributed mainly on the PXZ moieties.

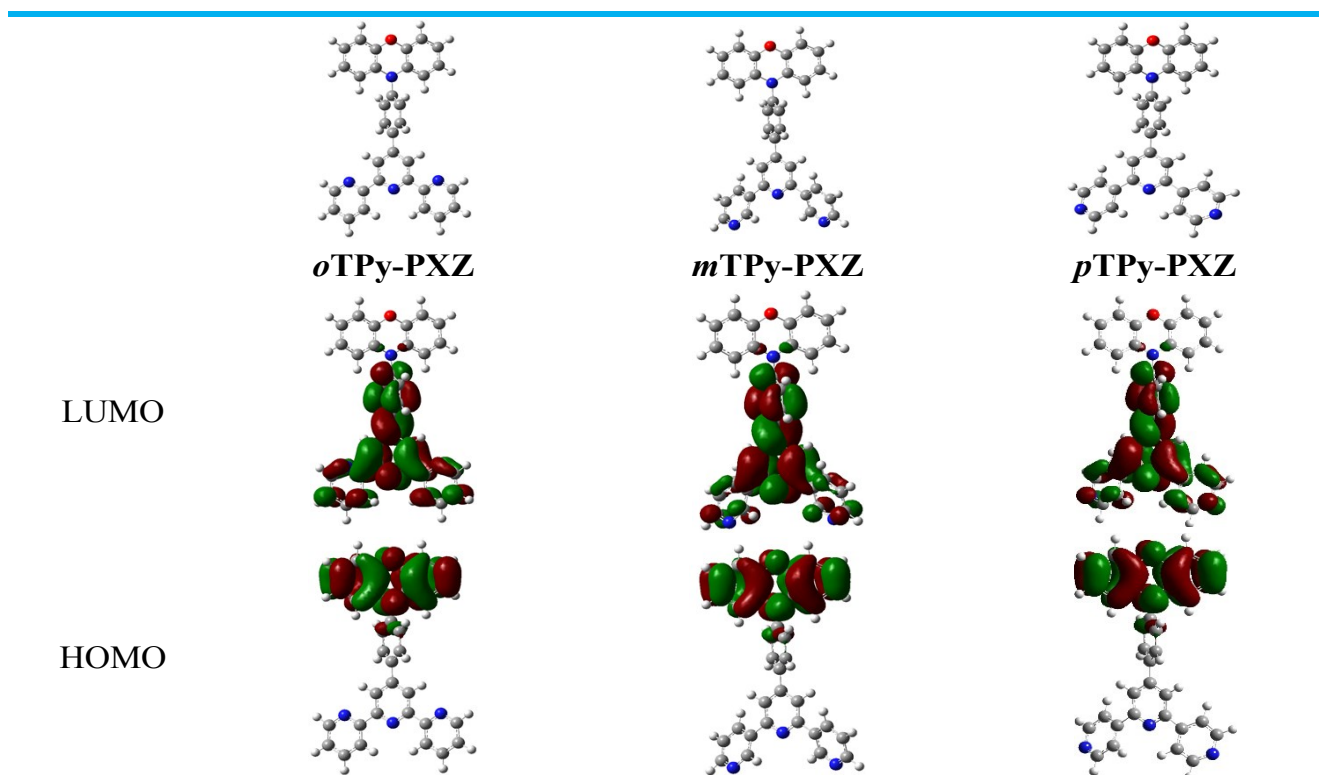


Fig. S1 Optimized ground molecular structures and the corresponding calculated spatial distributions of the frontier molecular orbitals (FMOs).

3.2 Photophysical properties

All three isomers show nearly identical UV-Vis absorption spectra in dilute toluene solution. The strong absorption bands around 320 nm can be ascribed to the $\pi-\pi^*$ transition from the PXZ or TPY units, while the weak absorption bands around 370 nm are derived from the intramolecular charge transfer (ICT) from PXZ to TPY moieties. Correspondingly, almost same broad and structureless photoluminescence spectra in toluene at room temperature are obtained. Thus, it can be concluded that all three emitters depict similar photophysical properties in dilute solution state.

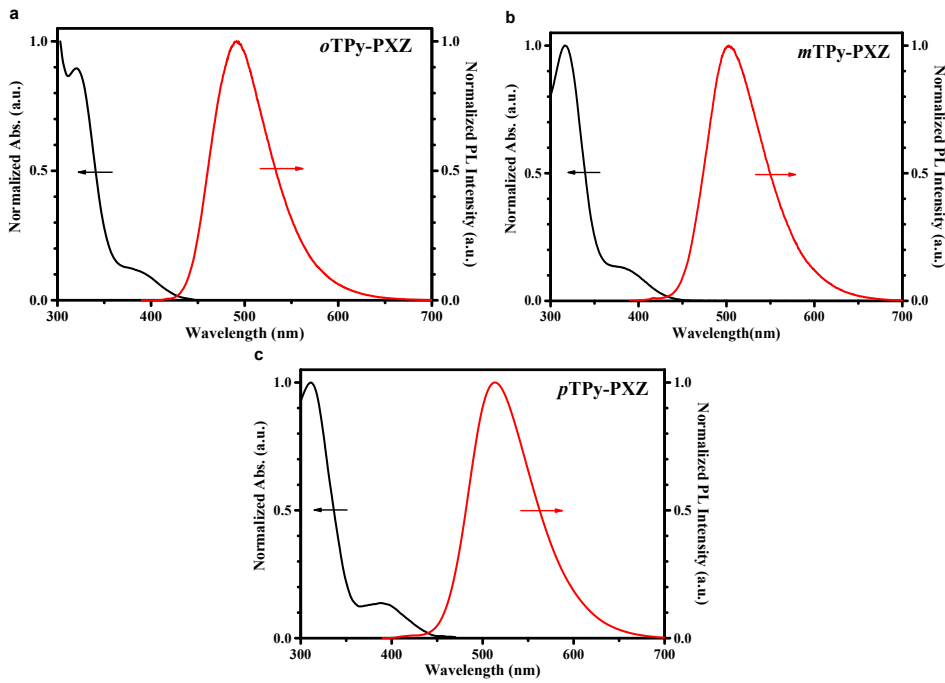


Fig. S2 Normalized UV–vis absorption (black) and fluorescence spectra (red) of a) *o*TPy-PXZ, b) *m*TPy-PXZ and c) *p*TPy-PXZ at r.t. in toluene.

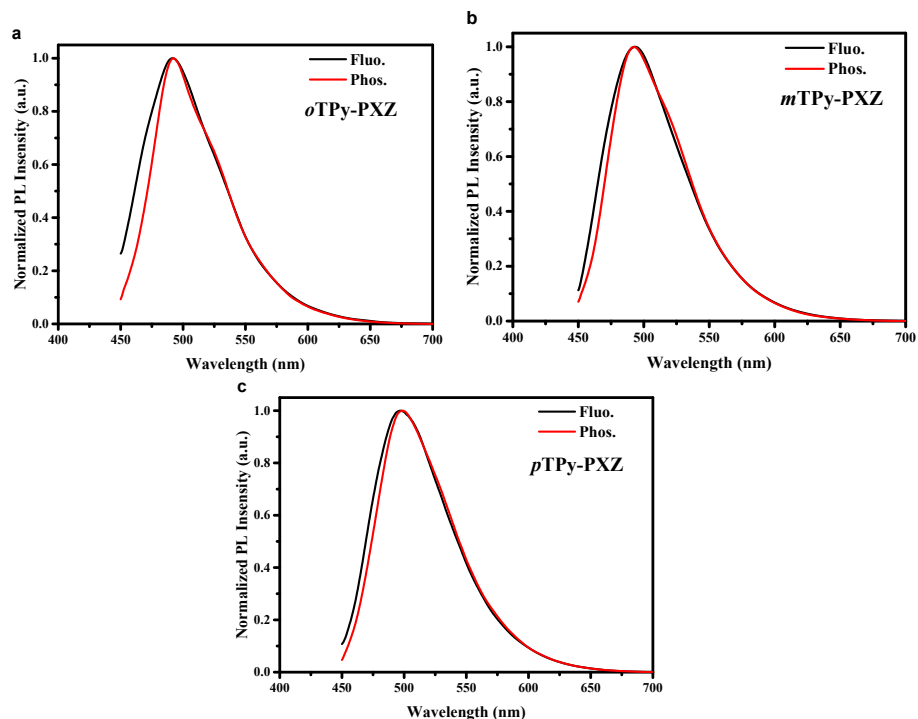


Fig. S3 Normalized fluorescence and phosphorescence spectra of a) *o*TPy-PXZ, b) *m*TPy-PXZ and c) *p*TPy-PXZ in 2-MeTHF at 77K.

3.3 Cyclic voltammograms

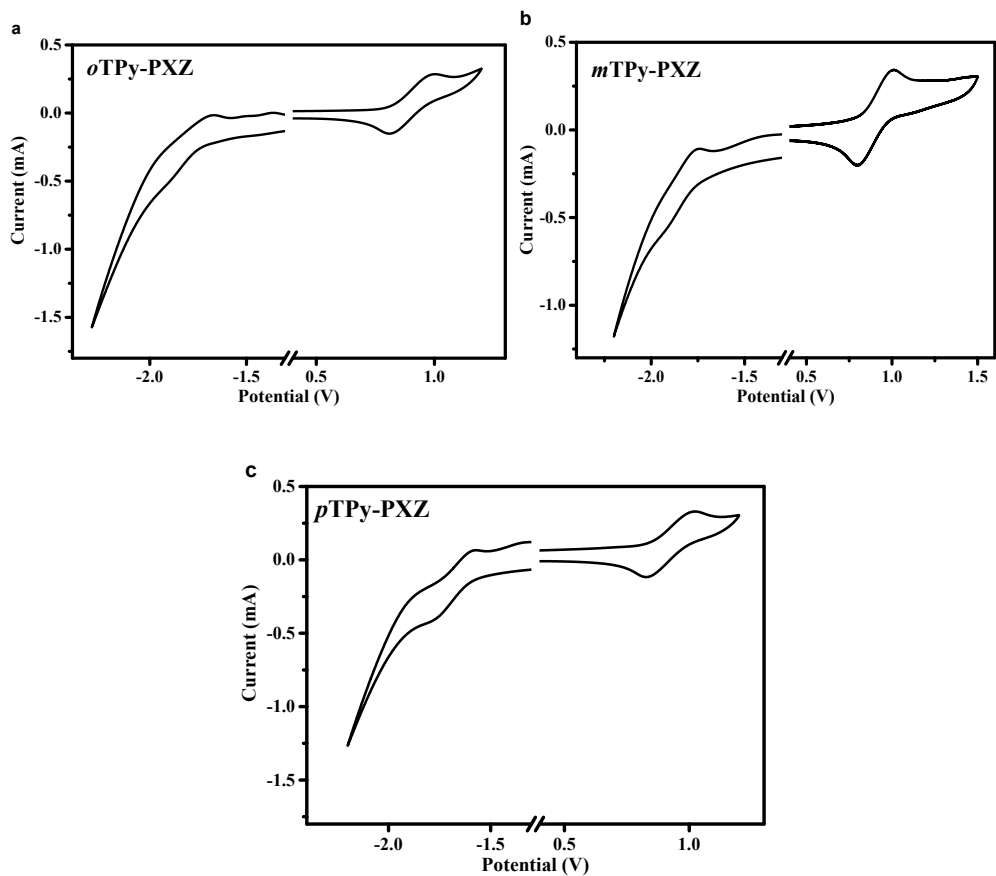


Fig. S4 Cyclic voltammograms of a) *o*TPy-PXZ, b) *m*TPy-PXZ and c) *p*TPy-PXZ.

3.4 Device configuration

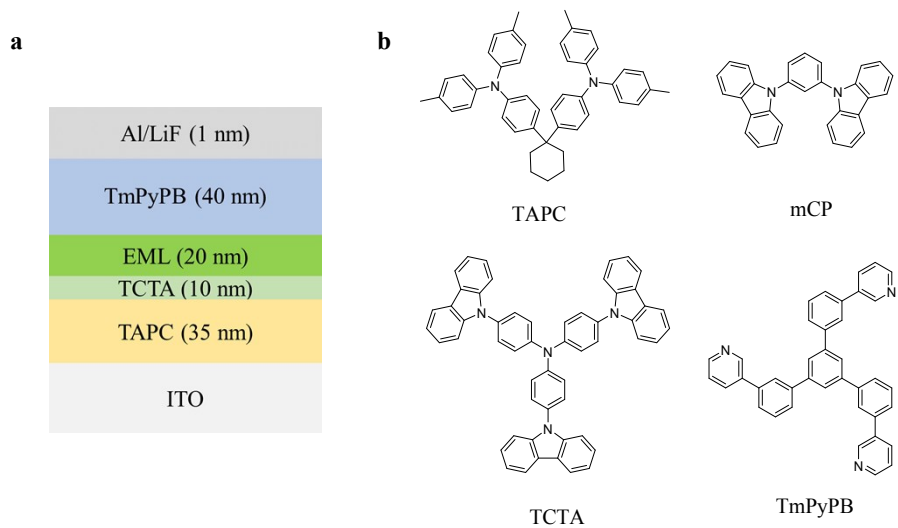


Fig. S5 a) Optimized OLED structures and b) the molecular structures employed in this work.

3.5 Single-crystal result

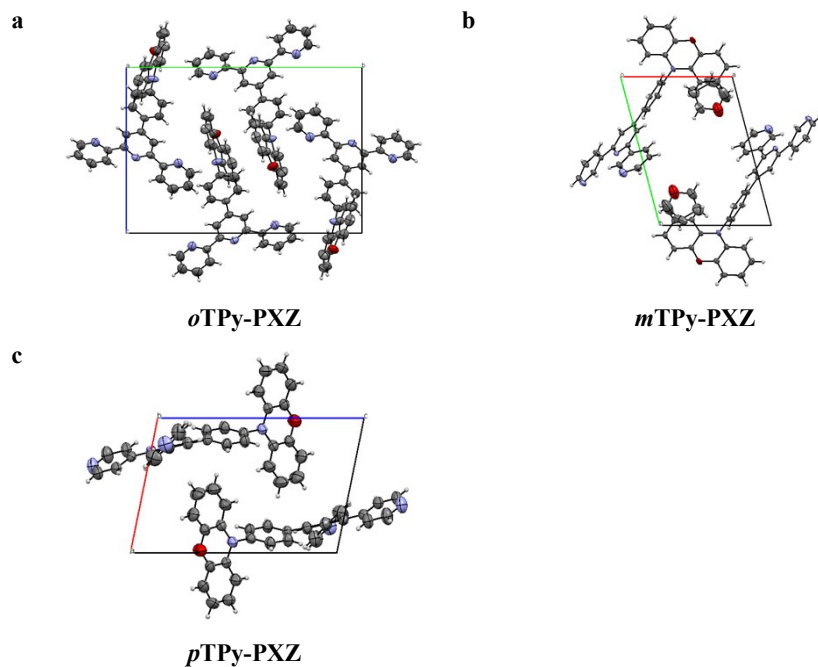


Fig. S6 Molecular packing modes determined from single crystals X-ray diffraction.

3.6 Spin density distributions (SDDs) of T₁ states

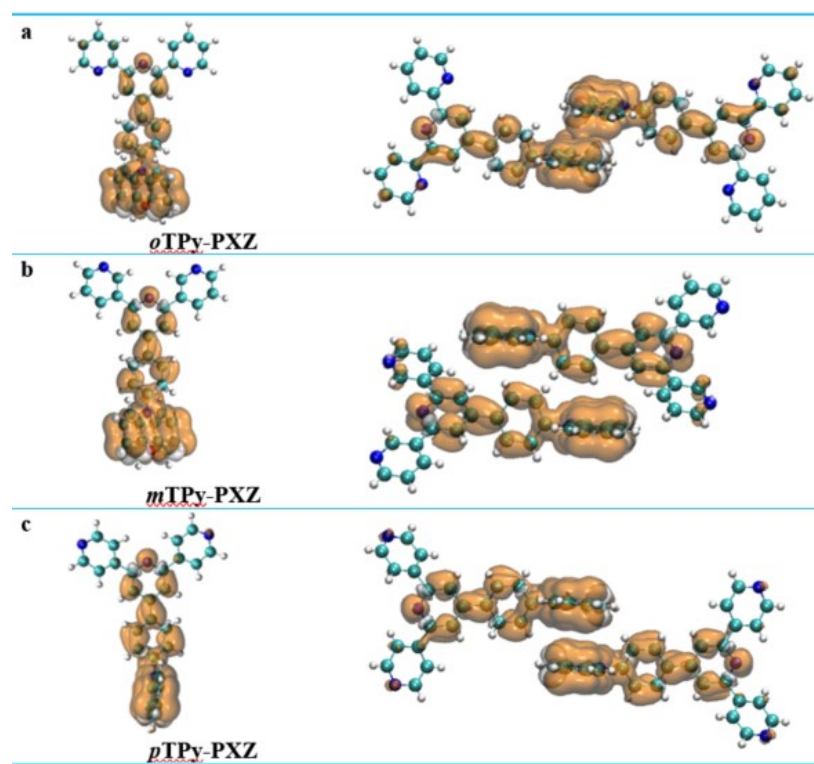


Fig. S7 Calculated spin density distributions of T₁ states in single-molecular state (left) and solid-state state (right) determined by single-crystal X-ray analysis. The isovalue is 0.0004.

3.7 Atomic force microscopy (AFM) and XRD patterns

The atomic force microscopy (AFM) was used to investigate the morphology of the films of the three isomers. The surface roughness of 40 nm-thick films vacuum deposited onto silicon substrate were observed using AFM in tapping mode. Unlike serious crystallinity issue of *o*TPy-PXZ and *p*TPy-PXZ, the neat film of *m*TPy-PXZ exhibits a negligible change of root-mean-square (rms) roughness (Rrms) after storage in ambient condition for two weeks,⁵ which fulfilled the requirement of film preparation via vacuum-deposition.

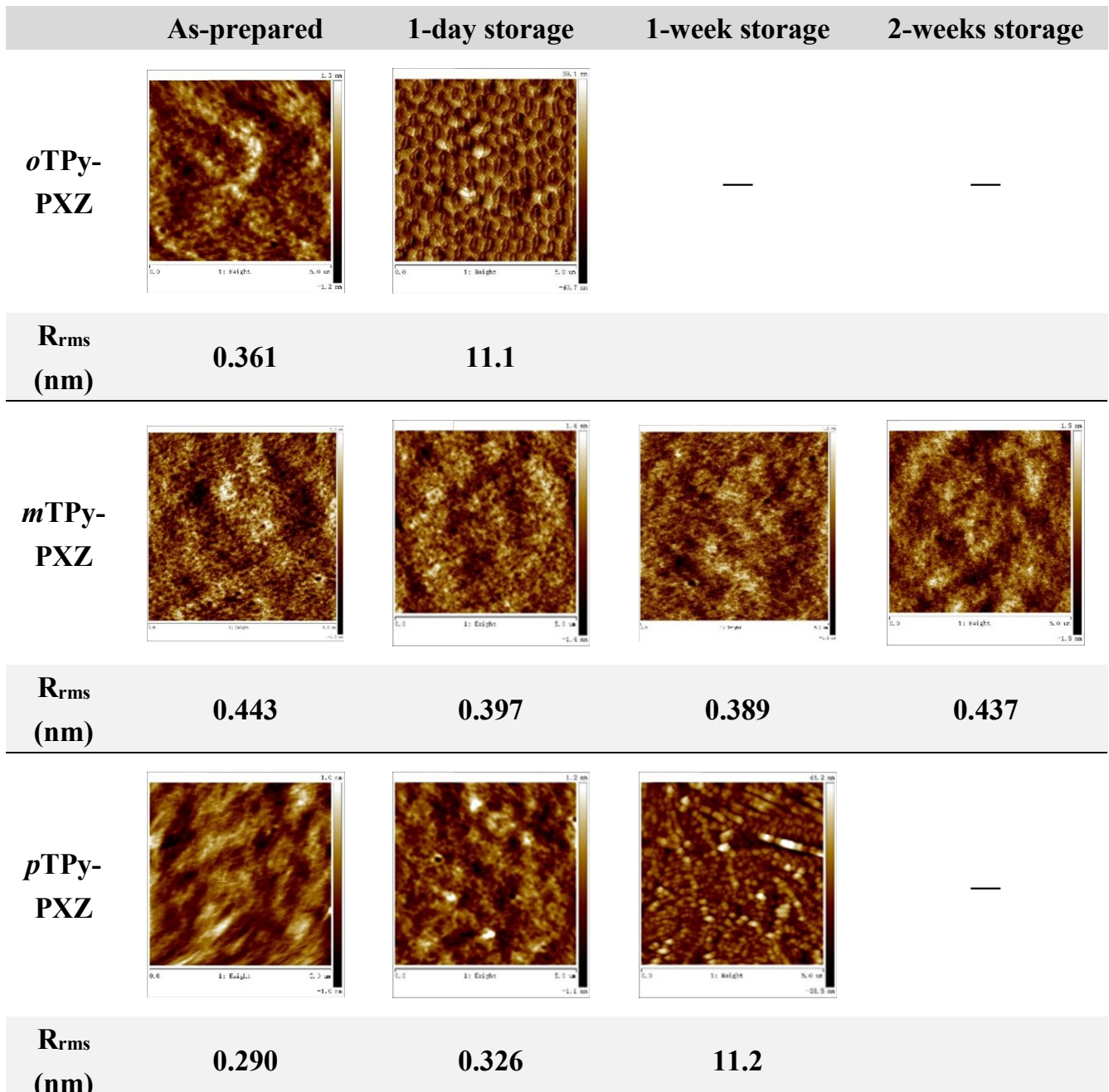


Fig. S8 AFM topographic images ($5 \times 5 \mu\text{m}$) and Rrms values of 40 nm-thick pristine films of TPy-based TADF emitters.

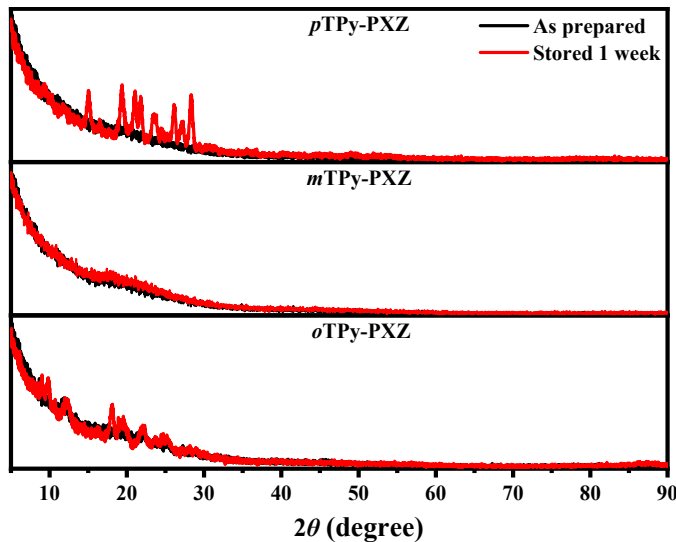


Fig. S9 XRD patterns of *p*TPy-PXZ, *m*TPy-PXZ and *o*TPy-PXZ films deposited on silicon substrate via thermal evaporation (black lines: as prepared; red lines: after storage for one week).

3.8 Carrier mobility

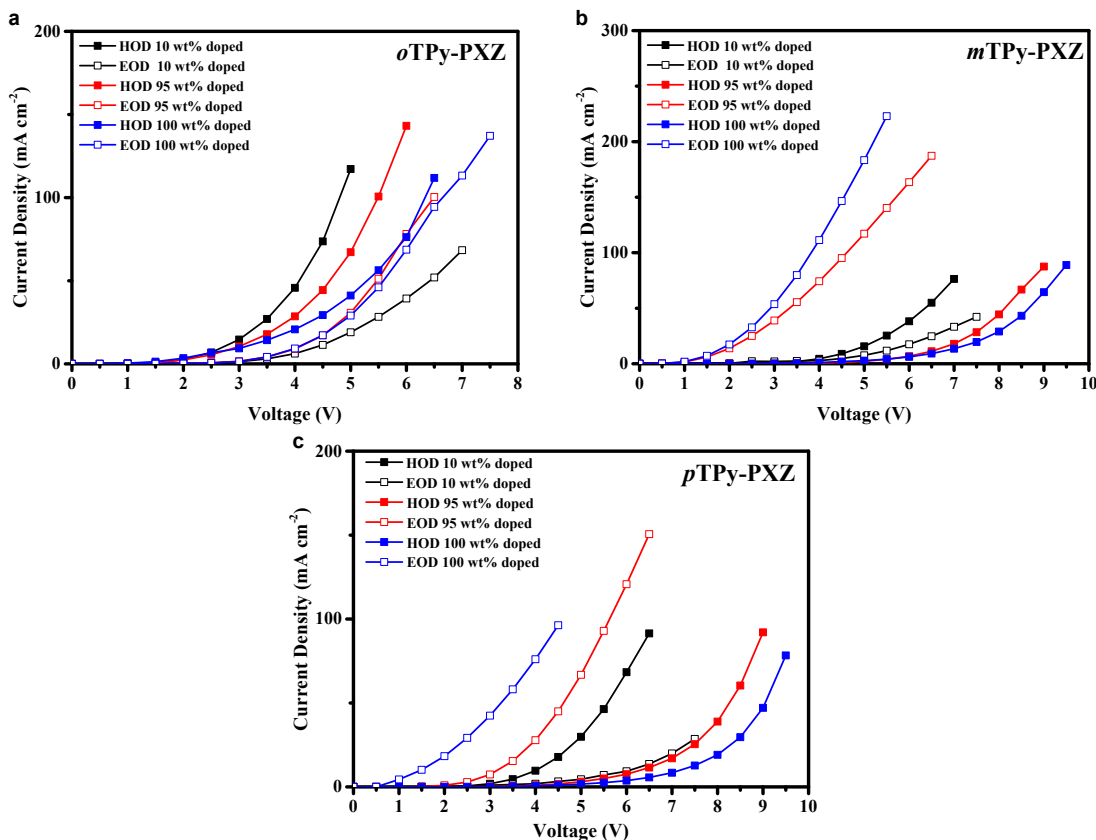


Fig. S10 Current density–Voltage characteristics of hole-only (HODs) and electron-only (EODs) devices for a) *o*TPy-PXZ, b) *m*TPy-PXZ and c) *p*TPy-PXZ 10 wt% (Black), 95 wt% (Red) and 100 wt% (Blue) doped in mCP. (HODs: ITO/ MoO₃ (12 nm)/ TPy-based emitters (30 nm)/ MoO₃ (12 nm)/ Al; EODs: ITO/ Al (40 nm)/ LiF (1 nm)/ TPy-based emitters (30 nm)/ LiF (1 nm)/ Al).

3.9 Transient PL measurements

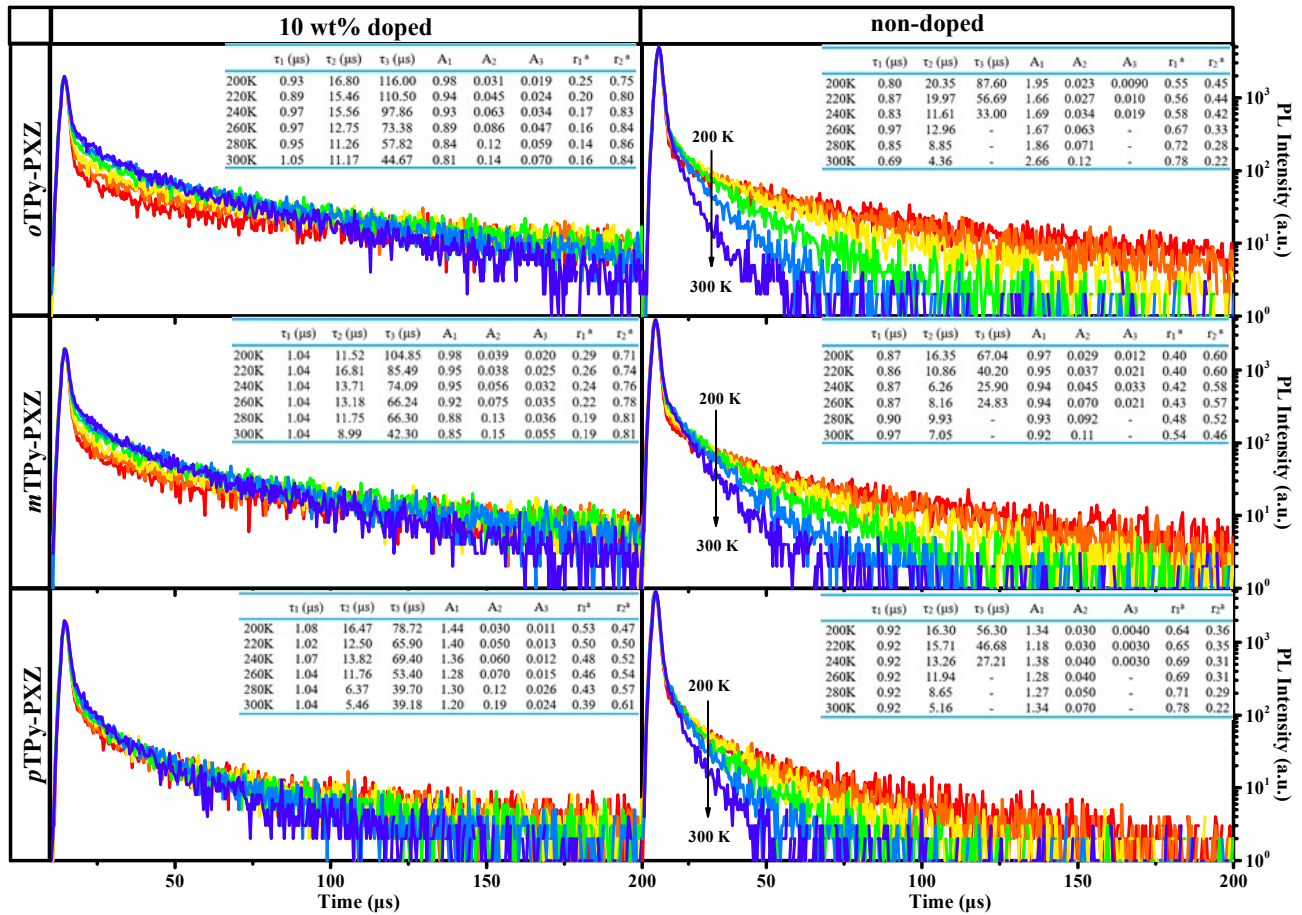


Fig. S11 Transient decay profiles of the 10 wt% doped in mCP and the neat films in time range of 200 μs at different temperatures (red, orange, yellow, green, blue and indigo for 200, 220, 240, 260, 280 and 300 K respectively) excited at 337 nm.(Inset: Obtained from the multi-exponential fitting of the transient decay curves on a 200 μs scale and corresponding intensity ratio between prompt (r_1) and delayed (r_2) components were determined using emission lifetime (τ_1 , τ_2 and τ_3) and fitting parameter (A_1 , A_2 and A_3) as the reported literature.⁶)

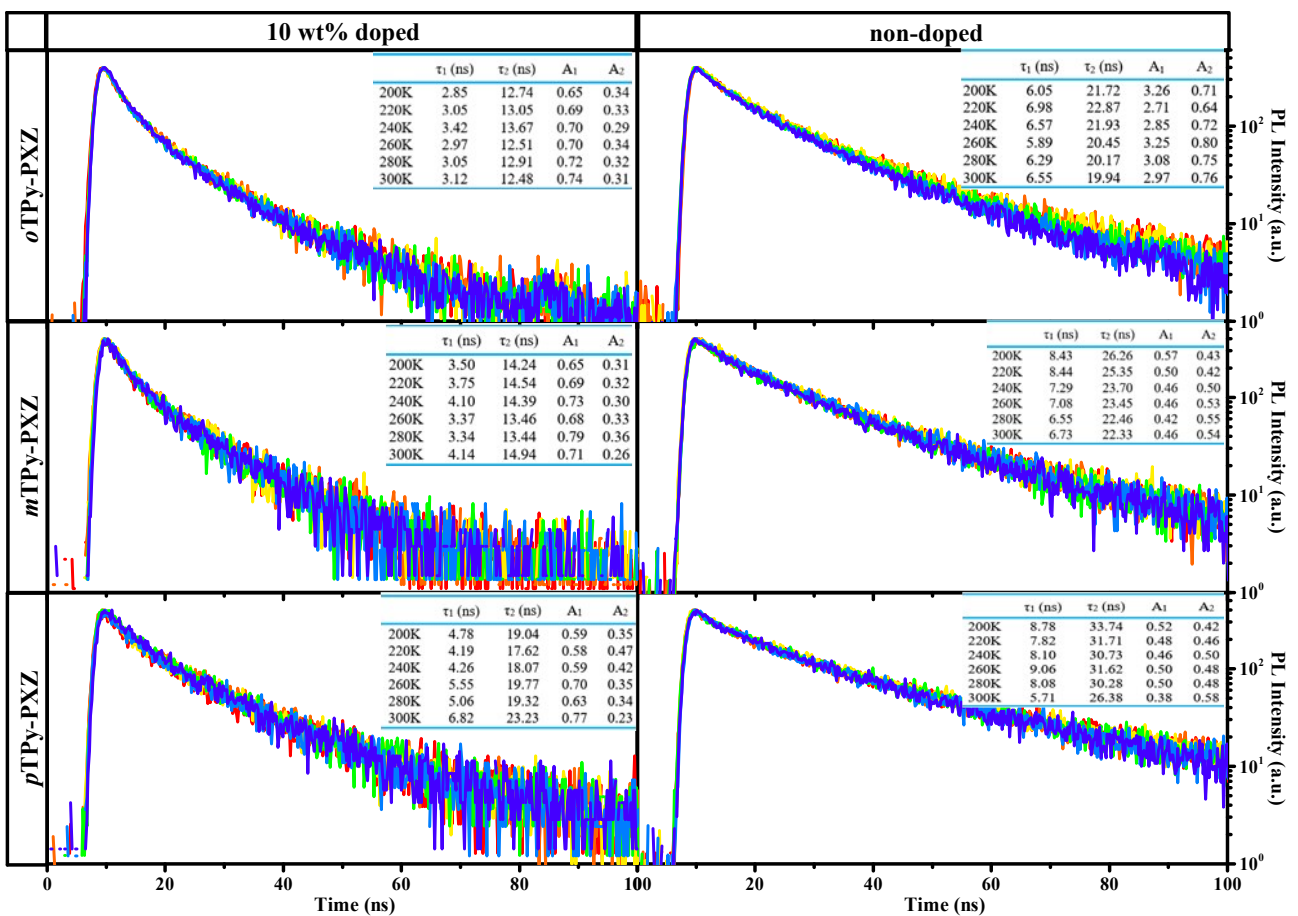


Fig. S12 Transient decay profiles of the 10 wt% doped in mCP and the neat films in time range of 100 ns at different temperatures (red, orange, yellow, green, blue and indigo for 200, 220, 240, 260, 280 and 300 K respectively) excited at 337 nm. (Insertion: Obtained from the multi-exponential fitting of the transient decay curves on a 100 ns scale)

The estimation was based on Arrhenius plot of $\ln k_{RISC} = -\Delta E_a^{TADF}/k_B T + \ln A$ where k_{RISC} , ΔE_a^{TADF} , A, k_B and T are the rate constant of reverse intersystem crossing (RISC) process, actual ΔE_{ST} , frequency factor, the Boltzmann's constant, and absolute temperature, respectively. Considering rate constant of intersystem crossing (ISC) process (k_{ISC}) is independent of temperature because ISC process is an adiabatic process, corresponding ΔE_a^{TADF} 's for the three isomers in 10 wt% doped and neat thin films can thus be estimated by the rewritten equation of $\ln(k_p k_d \phi_d / \phi_p) = -\Delta E_a^{TADF}/k_B T + \ln A + \ln k_{ISC}$.⁷ The three isomers display extremely small ΔE_a^{TADF} 's. Specifically, the ΔE_a^{TADF} 's in neat films are all estimated to be slight narrower than that of corresponding doped films, which can be attributed to the influence of different environmental polarity.

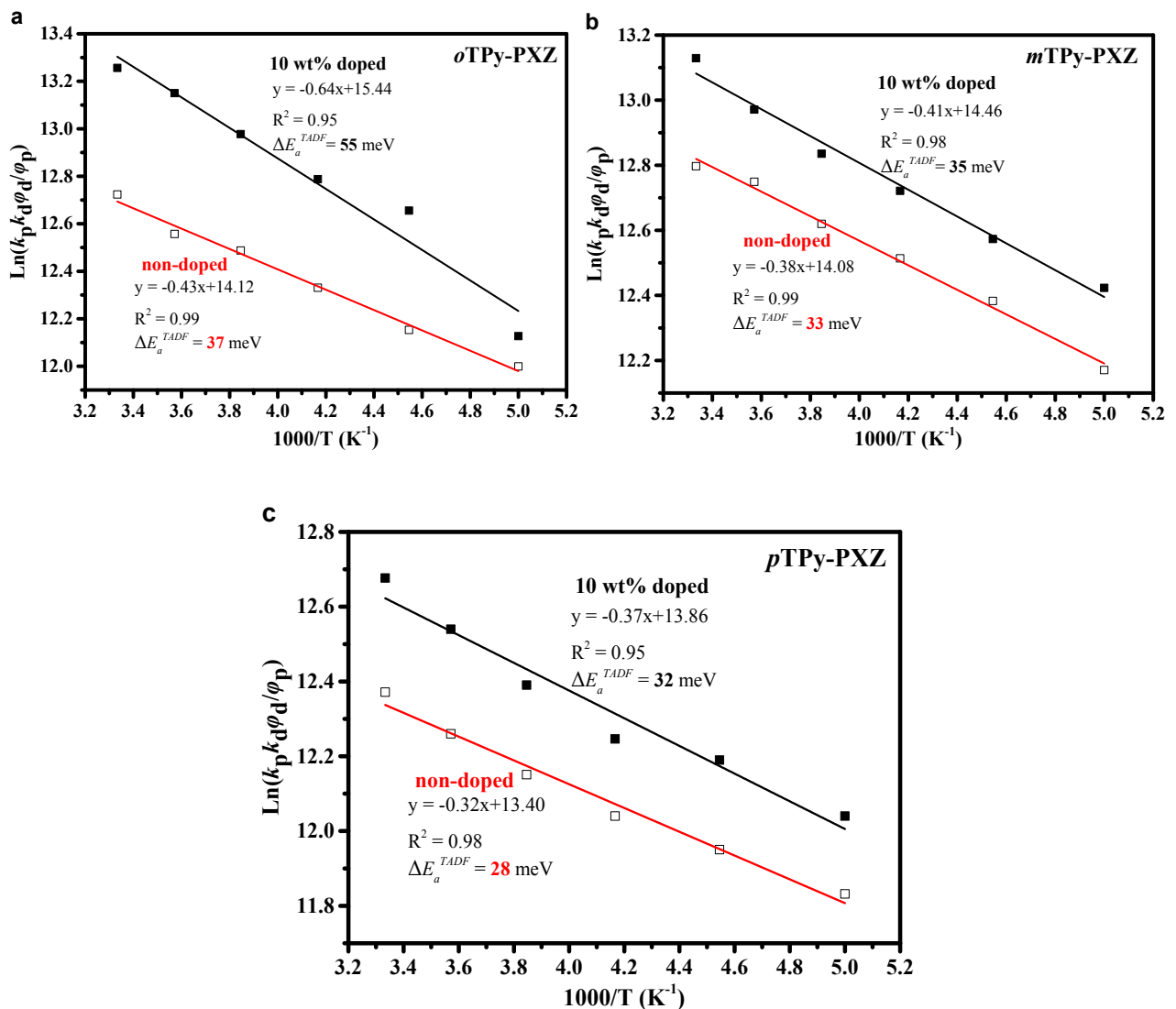


Fig. S13 $\ln(k_p k_d \phi_d / \phi_p)$ were plotted as a function of $1000/T$ of the three emitters 10 wt% doped (solid) and neat (hollow) films at different temperatures.

3.10 TTA model

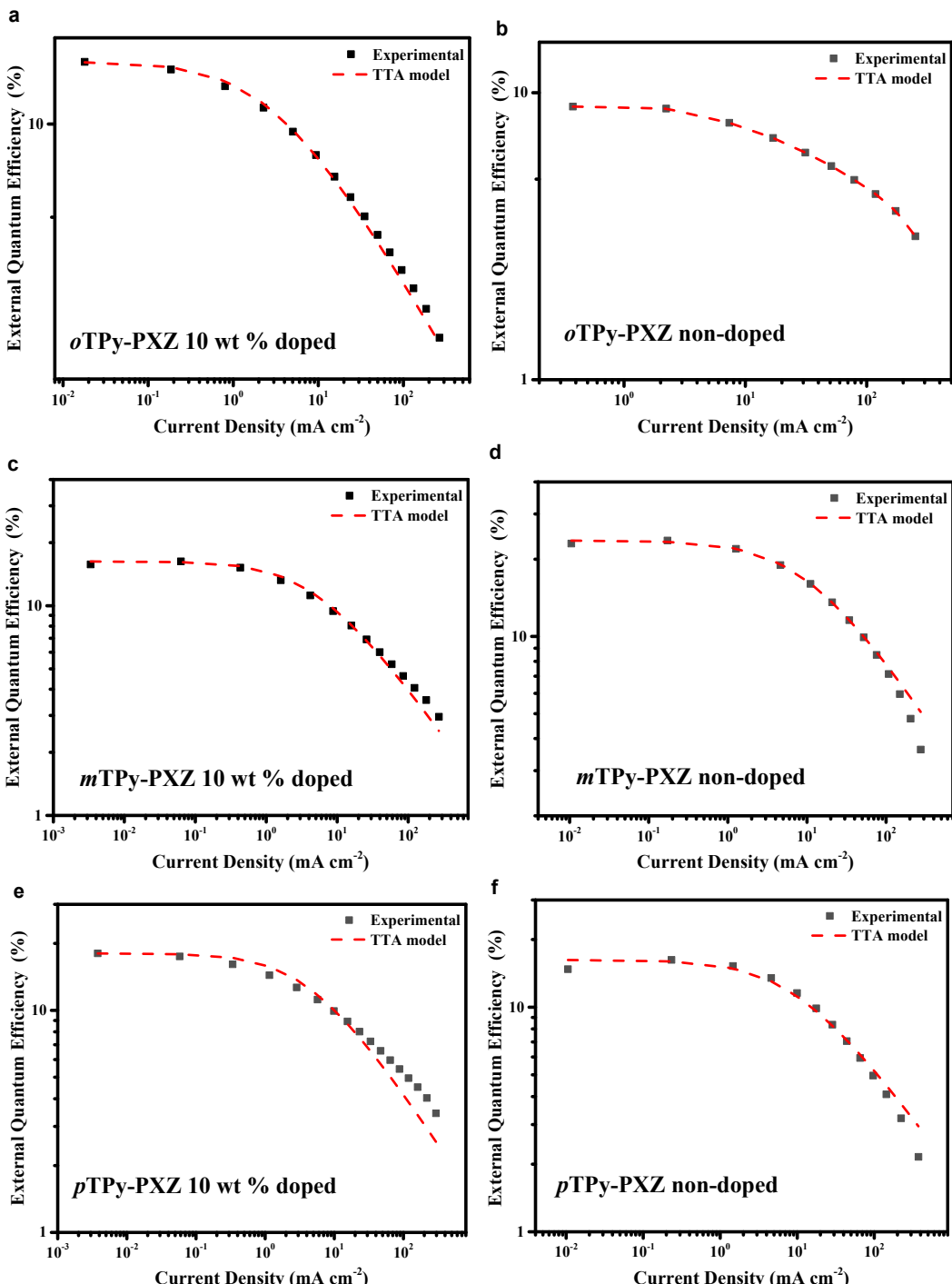


Fig. S14 EQE versus current density characteristics of terpyridine-based devices (a, c and e for *o*TPy-PXZ, *m*TPy-PXZ and *p*TPy-PXZ 10 wt% doped in mCP; b, d and f for *o*TPy-PXZ, *m*TPy-PXZ and *p*TPy-PXZ-based non-doped devices). The red dash lines represent the simulated results via the TTA model.^{8, 9}

3.11 Variable angle spectroscopic ellipsometry (VASE) measurement

A 70 nm thickness neat films of three isomers on a Si substrate were prepared by thermal evaporation and were measured with a spectroscopic ellipsometer (M-2000U, J. A. Woollam Co.Inc.) by varying the incident angles from 45° to 75° with steps of 5° . Anisotropic optical parameters, extinction coefficient (k) and refractive index (n) for the neat films were obtained by analyzing the experimental ellipsometric parameters Ψ and Δ using a uniaxial anisotropy model with Tauc-Lorentz-type and Gaussian-type oscillators via WVASE32 software (J. A. Woollam Co. Inc.). The orientation order parameter, S , were thus calculated from the equation ¹⁰: $S = (k_e - k_o)/(k_e + 2k_o)$. $S = -0.5$ if the molecules are completely parallel to the surfaces, $S = 0$ if they are randomly oriented, and $S = 1$ if they are completely perpendicular to the surface.¹¹ According to the VASE results, the horizontal orientation order parameter S are thus estimated to be -0.10 and -0.21 for *o*TPy-PXZ and *p*TPy-PXZ respectively.

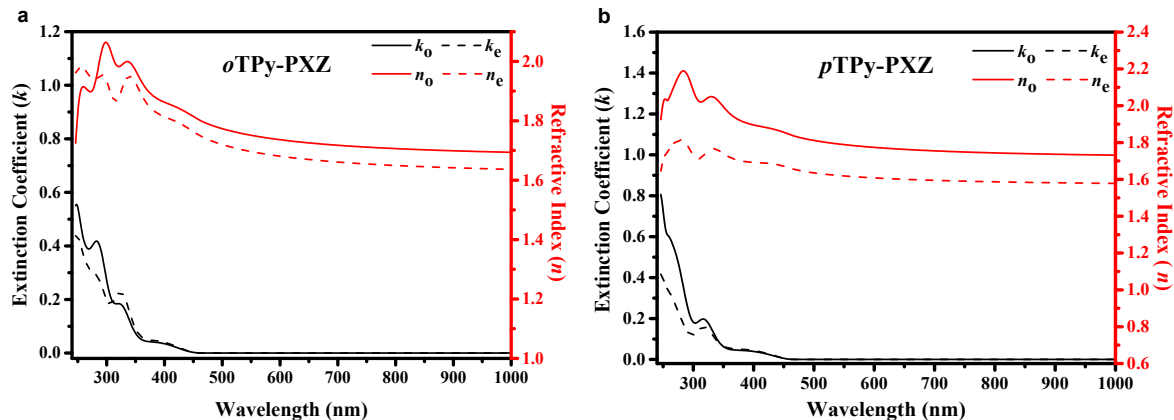


Fig. S15 Results of VASE measurements; extinction coefficient k (black) and refractive index n (red). The solid and dashed lines represent spectra for the ordinary (*o*) and extraordinary (*e*) optical constants of a) *o*TPy-PXZ and b) *p*TPy-PXZ.

3.12 NMR charts

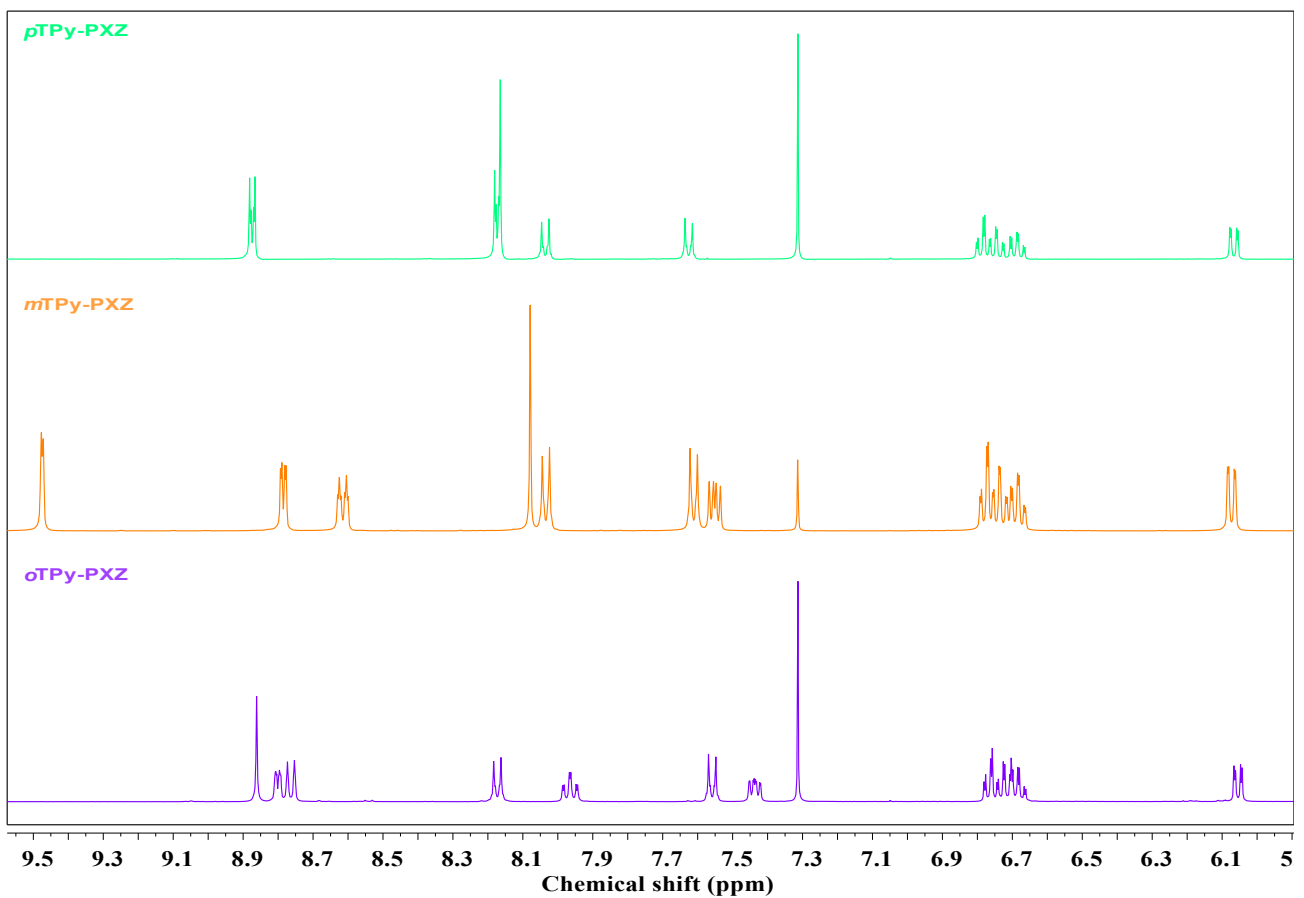


Fig. S16 ¹H NMR spectra of the three isomers (400 MHz, CDCl₃)

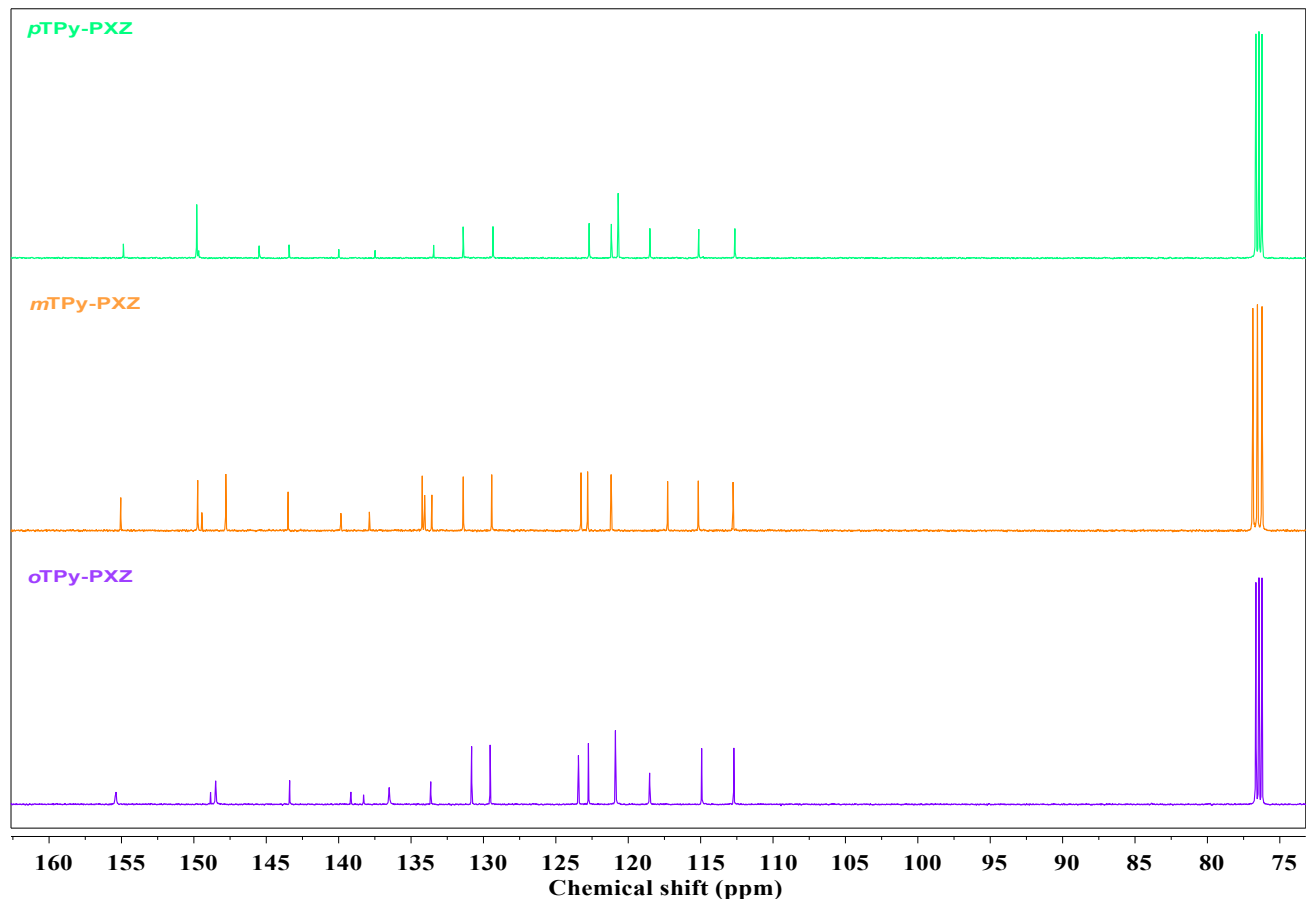
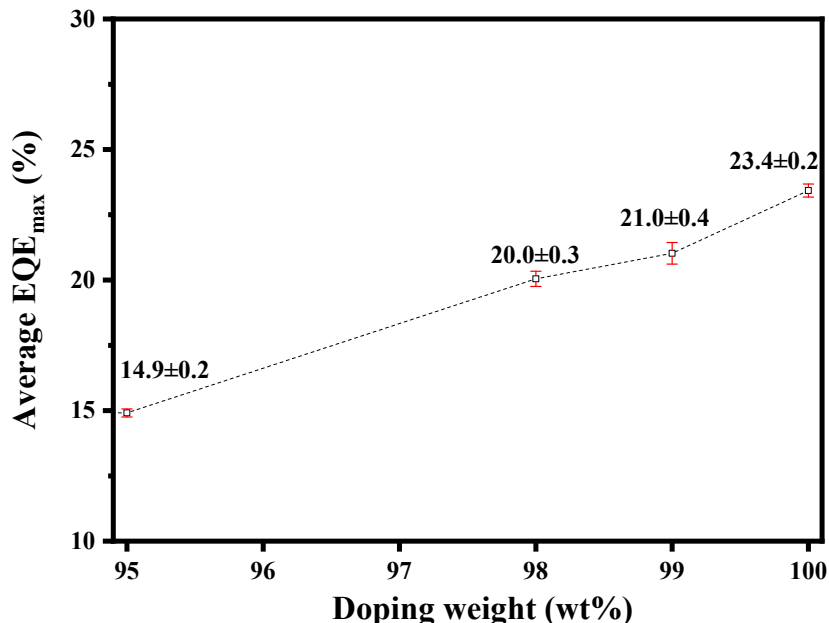


Fig. S17 ¹³C NMR spectra of the three isomers (101 MHz, CDCl₃)

Table S1 Electroluminescence properties of the three emitters.

Emitter	Doping weight (wt %)	$\lambda_{\text{Max.}}$ (nm)	$\text{CE}_{\text{Max}}/\text{PE}_{\text{Max}}/\text{EQE}_{\text{Max}}$ (cd·A⁻¹/ lm·W⁻¹/ %)	CIE (x, y)
<i>oTPy-PXZ</i>	5	500	40.6/41.1/14.3	(0.22,0.46)
	10	504	43.6/44.2/15.9	(0.24,0.48)
	20	512	46.9/46.0/15.7	(0.27,0.53)
	30	516	48.5/47.6/15.7	(0.29,0.55)
	50	520	42.2/41.5/13.4	(0.30,0.56)
	70	524	36.1/36.6/11.3	(0.31,0.56)
	95	528	29.5/28.7/9.2	(0.33,0.56)
	100	528	24.7/20.3/8.2	(0.33,0.56)
	5	500	44.2/44.8/15.5	(0.21,0.46)
	10	512	46.2/50.0/16.3	(0.25,0.51)
<i>mTPy-PXZ</i>	20	516	50.0/54.5/16.5	(0.27,0.53)
	27	516	57.6/60.3/19.1	(0.27,0.52)
	30	516	54.2/58.8/18.7	(0.27,0.53)
	50	526	52.5/53.2/16.4	(0.30,0.56)
	70	526	50.3/55.7/15.2	(0.30,0.56)
	95	532	49.5/54.7/15.0	(0.34,0.56)
	98	532	67.7/60.0/20.3	(0.34,0.56)
	99	532	71.4/74.5/21.3	(0.34,0.56)
	100	532	79.8/83.8/23.6	(0.34,0.56)
	5	508	50.4/51.1/15.7	(0.23,0.49)
<i>pTPy-PXZ</i>	10	516	55.3/62.0/18.0	(0.28,0.54)
	20	524	61.3/74.1/19.8	(0.31,0.57)
	21	524	62.7/70.3/20.2	(0.31,0.56)
	30	528	57.0/68.8/17.5	(0.33,0.57)
	50	536	56.0/67.6/17.0	(0.35,0.57)
	70	540	55.3/66.4/16.7	(0.38,0.57)
	95	540	52.9/60.4/16.2	(0.38,0.56)
	100	540	50.4/52.8/16.4	(0.38,0.55)

TAPC (35 nm)/TCTA (10 nm)/ EML (20 nm)/ TmPyPb (40 nm)/ LiF (1 nm)/ Al



<i>mTPy-PXZ</i> doping weight (wt %)	Average EQE_{Max} (%)	Standard deviation (%)	Best EQE_{Max} (%)
95	14.9	0.2	15.0
98	20.0	0.3	20.3
99	21.0	0.4	21.3
100	23.4	0.2	23.6

Fig. S18 Doping weight versus the average maximum EQE of *mTPy-PXZ*-based devices.

Table S2 Electroluminescence performances of the reported green to yellow TADF-based high-performance non-doped OLEDs.

Ref	Emitter	$\lambda_{\text{Max.}}$ [nm]	CE/ PE/ EQE [cd·A ⁻¹ / lm·W ⁻¹ / %]		EQE _{roll-off} ^a [%]	CIE (x, y)
			Maximum	@ 10 ³ cd·m ⁻²		
This work	<i>o</i> TPy-PXZ	528	24.7/20.3/8.2	23.6/17.2/7.6	7.3	(0.33, 0.56)
	<i>m</i>TPy-PXZ	532	79.8/83.8/23.6	74.1/72.7/21.9	7.2	(0.34, 0.56)
	<i>p</i> TPy-PXZ	540	50.4/52.8/16.4	43.5/34.1/14.1	14.0	(0.38, 0.55)
12	TCZPBOX	-	73.0/79.0/20.9	61.6/45.4/18.0	13.9	(0.40, 0.56)
13	2Cz-DPS	524	82.3/51.8/28.7	-/-/2.8	90.2	-
	4Cz-DPS	518	61.2/38.4/20.7	-/-/10.0	51.7	-
14	DspiroAc-TRZ	484	55.8/47.7/25.7	35.7/22.4/16.4	36.2	(0.18, 0.38)
15	DBT-BZ-DMAC	516	43.3/35.7/14.2	43.1/33.1/14.2	0.0	(0.26, 0.55)
16	DMAC-BP	510	-/-/18.9	-/-/18.0	4.8	(0.26, 0.55)
17	PTZ-XT	553	-/-/11.1	-	-	-
18	MPAc-BS	487	49.9/41.4/22.8	-/-/19.0	16.7	(0.15, 0.36)
19	TspiroS-TRZ	-	41.1/35.8/20.0	21.9/14.9/10.6	47.0	(0.16, 0.30)
20	CzDBA	560	-/-/19.0	-	-	-
21	4,4-CzSPz	526	61.2/38.4/20.7	30.2/16.0/10.3	50.2	-
22	DCB-BP-PXZ	548	72.9/81.8/22.6	-/-/22.0	2.8	(0.39,0.57)
	CBP-BP-PXZ	546	69.0/75.0/21.4	-/-/20.9	2.6	(0.39,0.57)
	mCP-BP-PXZ	542	72.3/79.0/22.1	-/-/21.5	2.9	(0.39,0.57)
	mCBP-BP-PXZ	542	70.4/76.5/21.8	-/-/21.5	1.0	(0.38,0.57)
23	CP-BZ-PXZ	554	46.1/55.7/15.3	38.4/30.2/12.7	17.0	(0.42,0.55)
	CP-BZ-PTZ	502	41.6/37.9/15.0	41.5/32.6/14.9	0.7	(0.23,0.49)
24	MeG2TAZ	510	26.5/21.5/9.4	-/-/7.1	24.5	-
	tBuG2TAZ	510	25.4/16.1/9.5	-/-/7.3	23.2	-
	PhG2TAZ	510	23.1/17.3/8.2	-/-/6.0	26.8	-
25	2CzSO	516	-/-/0.7	-	-	-
	3CzSO	528	-/-/7.3	-	-	-
26	PAPCC	521	41.8/37.1/12.6	-	-	(0.30,0.59)
	PAPTC	508	3.6/3.7/1.3	-	-	(0.25,0.47)
27	PABPC0.5	-	36.2/339/10.7	28.8/19.6/8.5	20.6	(0.36, 0.57)
	PABPC1	-	52.3/53.5/15.4	48.2/38.9/14.2	7.8	(0.36, 0.57)
	PABPC5	-	60.5/61.2/18.1	59.4/50.4/17.8	1.6	(0.40, 0.56)
	PABPC10	-	55.1/54.4/16.2	54.5/42.8/16.0	1.2	(0.40, 0.56)

^aEQE_{roll-off} = (EQE_{max}-EQE₁₀₀₀)/EQE_{max}

For a TADF system, the main exciton loss channels are either singlet or triplet nonradiative transition processes. In blue-green emission range with small ΔE_{ST} , the rate constant of singlet nonradiative transition process (k_{nr}^S) is generally far lower than that of singlet radiative process (k_r^S) and ISC process and thus can be ignored. Herein to simplify the analysis, we attributed the triplet nonradiative transition process as the only considered exciton loss route. The key kinetic parameters of 10 wt% doped and neat films of three TADF emitters are estimated according the following equations and the key kinetic parameters are summarized in Table S4.^{28,29}

$$k_p = \frac{1}{\tau_p}; \quad k_d = \frac{1}{\tau_d};$$

$$k_r^S = k_p \phi_p; \quad k_{ISC} = k_p (1 - \phi_p);$$

$$k_{RISC} = \frac{k_p k_d \phi_d}{k_{ISC} \phi_p}; \quad k_{nr}^T = k_d - \left(1 - \frac{k_{ISC}}{k_p}\right) k_{RISC}$$

Table S3 Detailed photophysical properties and rate constants from 200 to 300 K.

Emitter	EML	T [K]	ϕ	ϕ_p	ϕ_d	k_p [10 ⁷ s ⁻¹]	k_d [10 ⁴ s ⁻¹]
<i>oTPy-PXZ</i>	10 wt% doped in mCP	200	0.70	0.18	0.53	10.22	1.03
		220	0.69	0.14	0.55	10.26	1.10
		240	0.68	0.12	0.56	10.23	1.26
		260	0.67	0.11	0.56	10.64	1.70
		280	0.67	0.10	0.57	10.53	2.24
		300	0.67	0.10	0.57	11.17	2.97
	non-doped	200	0.72	0.40	0.32	7.73	1.60
		220	0.71	0.40	0.31	7.18	2.56
		240	0.67	0.39	0.28	7.37	4.05
		260	0.61	0.41	0.20	7.93	7.72
		280	0.56	0.40	0.16	8.09	11.30
		300	0.52	0.40	0.12	8.05	22.93
<i>mTPy-PXZ</i>	10 wt% doped in mCP	200	0.76	0.22	0.54	9.46	1.13
		220	0.77	0.20	0.57	9.35	1.44
		240	0.75	0.18	0.57	9.86	1.69
		260	0.73	0.16	0.57	9.97	1.99
		280	0.73	0.14	0.59	10.11	2.20
		300	0.75	0.14	0.61	9.77	3.32
	non-doped	200	0.85	0.34	0.51	4.78	2.08
		220	0.85	0.34	0.51	4.85	3.25
		240	0.85	0.36	0.49	4.97	4.75
		260	0.83	0.35	0.48	4.98	6.18
		280	0.83	0.40	0.43	5.11	10.07
		300	0.82	0.45	0.38	5.22	14.18
<i>pTPy-PXZ</i>	10 wt% doped in mCP	200	0.98	0.52	0.46	6.78	1.82
		220	0.97	0.48	0.49	6.86	2.22
		240	0.97	0.46	0.51	6.85	2.34
		260	0.94	0.43	0.51	6.81	3.04
		280	0.94	0.41	0.53	6.80	3.90
		300	0.93	0.37	0.56	6.61	4.64
	non-doped	200	0.78	0.50	0.28	3.62	3.39
		220	0.76	0.49	0.27	3.73	4.35
		240	0.73	0.51	0.22	3.80	6.54
		260	0.69	0.48	0.21	3.79	8.38
		280	0.66	0.47	0.19	3.93	11.56
		300	0.64	0.50	0.14	4.20	19.39

Table S4 summary of kinetic parameters of the three emitters at 300 K.

EML		ϕ^a	ϕ_p^b	ϕ_d^b	τ_p^c [ns]	τ_d^c [μs]	k_r^S [10 ⁷ s ⁻¹]	k_{ISC} [10 ⁷ s ⁻¹]	k_{RISC} [10 ⁵ s ⁻¹]	k_{nr}^T [10 ⁴ s ⁻¹]
<i>o</i> TPy-PXZ	10 wt% doped	0.67	0.11	0.56	8.95	33.66	1.16	10.01	1.80	1.09
	non-doped	0.52	0.41	0.11	12.43	4.36	3.25	4.79	1.10	18.48
<i>m</i> TPy-PXZ	10 wt% doped	0.75	0.14	0.61	10.24	30.13	1.42	8.35	1.61	0.98
	non-doped	0.82	0.44	0.38	19.14	7.05	2.33	2.90	2.16	4.55
<i>p</i> TPy-PXZ	10 wt% doped	0.93	0.36	0.57	15.12	21.54	2.41	4.20	1.13	0.51
	non-doped	0.64	0.50	0.14	23.80	5.16	2.09	2.11	1.11	13.87

^aAbsolute PL quantum yield evaluated using an integrating sphere of all three emitters 10 wt% doped in mCP and nond-doped films under nitrogen conditions. ^bDetermined from the ratio of prompt (r_1) and delayed (r_2) components in transient decay. ^cAverage lifetime calculated by $\tau = \sum A_i \tau_i^2 / \sum A_i \tau_i$.³⁰

4. References

1. E. Runge and E. K. U. Gross, *Phys. Rev. Lett.*, 1984, **52**, 997-1000.
2. A. D. Boese and J. M. Martin, *J. Chem. Phys.*, 2004, **121**, 3405-3416.
3. T. Lu and F. Chen, *J. Comput. Chem.*, 2012, **33**, 580-592.
4. C.-L. Liu, C.-J. Zheng, X.-K. Liu, Z. Chen, J.-P. Yang, F. Li, X.-M. Ou and X.-H. Zhang, *J. Mater. Chem. C*, 2015, **3**, 1068-1076.
5. Y. Watanabe, R. Yoshioka, H. Sasabe, T. Kamata, H. Katagiri, D. Yokoyama and J. Kido, *J. Mater. Chem. C*, 2016, **4**, 8980-8988.
6. T. Nakagawa, S.-Y. Ku, K.-T. Wong and C. Adachi, *Chem. Commun.*, 2012, **48**, 9580-9582.
7. R. Ishimatsu, S. Matsunami, K. Shizu, C. Adachi, K. Nakano and T. Imato, *J. Phys. Chem. A*, 2013, **117**, 5607-5612.
8. C. Murawski, K. Leo and M. C. Gather, *Adv. Mater.*, 2013, **25**, 6801-6827.
9. X. Li, Y. Z. Shi, K. Wang, M. Zhang, C. J. Zheng, D. M. Sun, G. L. Dai, X. C. Fan, D. Q. Wang, W. Liu, Y. Q. Li, J. Yu, X. M. Ou, C. Adachi and X. H. Zhang, *ACS Appl. Mater. Interfaces*, 2019, **11**, 13472-13480.
10. H. Kaji, H. Suzuki, T. Fukushima, K. Shizu, K. Suzuki, S. Kubo, T. Komino, H. Oiwa, F. Suzuki, A. Wakamiya, Y. Murata and C. Adachi, *Nat. Commun.*, 2015, **6**, 8476-8483.
11. D. Yokoyama, A. Sakaguchi, M. Suzuki and C. Adachi, *Appl. Phys. Lett.*, 2008, **93**, 173302-173304.
12. X. Zhang, M. W. Cooper, Y. Zhang, C. Fuentes-Hernandez, S. Barlow, S. R. Marder and B. Kippelen, *ACS Appl. Mater. Interfaces*, 2019, **11**, 12693-12698.
13. Z. Yang, Z. Mao, C. Xu, X. Chen, J. Zhao, Z. Yang, Y. Zhang, W. Wu, S. Jiao, Y. Liu, M. P. Aldred and Z. Chi, *Chem. Sci.*, 2019, **10**, 8129-8134.
14. W. Li, W. Li, L. Gan, M. Li, N. Zheng, C. Ning, D. Chen, Y. C. Wu and S. J. Su, *ACS Appl. Mater. Interfaces*, 2020, **12**, 2717-2723.
15. J. Guo, X.-L. Li, H. Nie, W. Luo, S. Gan, S. Hu, R. Hu, A. Qin, Z. Zhao, S.-J. Su and B. Z. Tang, *Adv. Funct. Mater.*, 2017, **27**, 1606458.
16. Q. Zhang, D. Tsang, H. Kuwabara, Y. Hatae, B. Li, T. Takahashi, S. Y. Lee, T. Yasuda and

- C. Adachi, *Adv. Mater.*, 2015, **27**, 2096-2100.
17. N. Aizawa, C.-J. Tsou, I. S. Park and T. Yasuda, *Polym J.*, 2016, **49**, 197-202.
18. I. S. Park, K. Matsuo, N. Aizawa and T. Yasuda, *Adv. Funct. Mater.*, 2018, **28**, 1802031.
19. W. Li, B. Li, X. Cai, L. Gan, Z. Xu, W. Li, K. Liu, D. Chen and S. J. Su, *Angew. Chem. Int. Ed.*, 2019, **58**, 11301-11305.
20. N. B. Kotadiya, P. W. M. Blom and G.-J. A. H. Wetzelaer, *Nat. Photon.*, 2019, **13**, 765-769.
21. J. Zhao, X. Chen, Z. Yang, T. Liu, Z. Yang, Y. Zhang, J. Xu and Z. Chi, *J. Phys. Chem. C*, 2019, **123**, 1015-1020.
22. H. Liu, J. Zeng, J. Guo, H. Nie, Z. Zhao and B. Z. Tang, *Angew. Chem. Int. Ed.*, 2018, **57**, 9290-9294.
23. J. Huang, H. Nie, J. Zeng, Z. Zhuang, S. Gan, Y. Cai, J. Guo, S. J. Su, Z. Zhao and B. Z. Tang, *Angew. Chem. Int. Ed.*, 2017, **56**, 12971-12976.
24. K. Albrecht, K. Matsuoka, D. Yokoyama, Y. Sakai, A. Nakayama, K. Fujita and K. Yamamoto, *Chem. Commun.*, 2017, **53**, 2439-2442.
25. Y. Li, T. Chen, M. Huang, y. gu, S. Gong, G. Xie and C. Yang, *J. Mater. Chem. C*, 2017, **5**, 3480-3487
26. Y. Zhu, Y. Zhang, B. Yao, Y. Wang, Z. Zhang, H. Zhan, B. Zhang, Z. Xie, Y. Wang and Y. Cheng, *Macromolecules*, 2016, **49**, 4373-4377.
27. Y. Yang, S. Wang, Y. Zhu, Y. Wang, H. Zhan and Y. Cheng, *Adv. Funct. Mater.*, 2018, **28**, 1706916.
28. K. Wang, W. Liu, C. J. Zheng, Y. Z. shi, K. Liang, M. Zhang, X. M. Ou and X. H. Zhang, *J. Mater. Chem. C*, 2017, **5**, 4797-4803.
29. K. Masui, H. Nakanotani and C. Adachi, *Org. Electron.*, 2013, **14**, 2721-2726.
30. Q. Zhang, H. Kuwabara, W. J. Potscavage, S. Huang, Y. Hatae, T. Shibata and C. Adachi, *J. Am. Chem. Soc.*, 2014, **136**, 18070-18081.